Journal of Colloid and Interface Science 513 (2018) 141–150

Contents lists available at ScienceDirect

Journal of Colloid and Interface Science

journal homepage: www.elsevier.com/locate/jcis

Regular Article

Membrane interactions of microgels as carriers of antimicrobial peptides

Randi Nordström [a,*], Lina Nyström [a], Oliver C.J. Andrén [b], Michael Malkoch [b], Anita Umerska [c], Mina Davoudi [d], Artur Schmidtchen [d,e], Martin Malmsten [a,f]

[a] Department of Pharmacy, Uppsala University, SE-75123 Uppsala, Sweden
[b] Department of Fibre & Polymer Technology, Royal Institute of Technology, SE-10044 Stockholm, Sweden
[c] MINT, UNIV Angers, INSERM U1066, CNRS 6021, Université Bretagne Loire, Angers Cedex, France
[d] Division of Dermatology and Venereology, Department of Clinical Sciences, Lund University, SE-22184 Lund, Sweden
[e] Lee Kong Chian School of Medicine, Nanyang Technological University, 11 Mandalay Road, Singapore 308232, Singapore
[f] Department of Pharmacy, University of Copenhagen, DK-2100 Copenhagen, Denmark

GRAPHICAL ABSTRACT

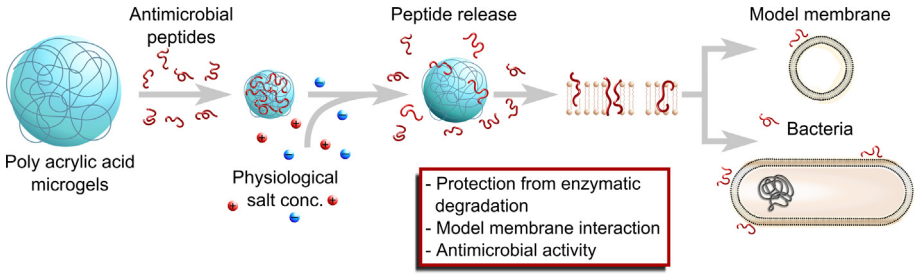

ARTICLE INFO

Article history:
Received 27 September 2017
Revised 1 November 2017
Accepted 4 November 2017
Available online 6 November 2017

Keywords:
Antimicrobial peptide
Drug delivery
Lipid membrane
Microgel

ABSTRACT

Microgels are interesting as potential delivery systems for antimicrobial peptides. In order to elucidate membrane interactions of such systems, we here investigate effects of microgel charge density on antimicrobial peptide loading and release, as well as consequences of this for membrane interactions and antimicrobial effects, using ellipsometry, circular dichroism spectroscopy, nanoparticle tracking analysis, dynamic light scattering and z-potential measurements. Anionic poly(ethyl acrylate-*co*-methacrylic acid) microgels were found to incorporate considerable amounts of the cationic antimicrobial peptides LL-37 (LLGDFFRKSKEKIGKEFKRIVQRIKDFLRNLVPRTES) and DPK-060 (GKHKNKGKKNGKHNGWKWWW) and to protect incorporated peptides from degradation by infection-related proteases at high microgel charge density. As a result of their net negative z-potential also at high peptide loading, neither empty nor peptide-loaded microgels adsorb at supported bacteria-mimicking membranes. Instead, membrane disruption is mediated almost exclusively by peptide release. Mirroring this, antimicrobial effects against several clinically relevant bacteria (*methicillin-resistant Staphylococcus aureus* (MRSA), *Escherichia coli*, and *Pseudomonas aeruginosa*) were found to be promoted by factors facilitating peptide release, such as decreasing peptide length and decreasing microgel charge density. Microgels were further demonstrated to display low toxicity towards erythrocytes. Taken together, the results demonstrate some interesting opportunities for the use of microgels as delivery systems for antimicrobial peptides, but also highlight several key factors which need to be controlled for their successful use.

* Corresponding author.
E-mail address: randi.nordstrom@farmaci.uu.se (R. Nordström).

https://doi.org/10.1016/j.jcis.2017.11.014
0021-9797/

1. Introduction

Due to increasing resistance against conventional antibiotics, antimicrobial peptides (AMPs) have received considerable attention as potential therapeutics. Although AMPs affect bacteria in numerous ways, their main mode of action is through direct membrane rupture, providing them with fast and broad-spectrum antimicrobial effects [1–3]. Through various approaches, such as combinatory library approaches [4], quantitative structure-activity relationship studies [5,6], identification of endogenous peptides derived from infection-related proteolysis [7], and end-tagging with short tryptophan or phenylalanine stretches [8], AMPs have been designed to display high potency, also against demanding (e.g., antibiotics-resistant) bacteria, yet displaying low toxicity against human cells. In addition to direct antimicrobial effects, some AMPs also display other host defense properties, including anti-inflammatory [2,9] and anticancer [10] effects. These effects are again depending on AMP interactions with membranes and membrane components, but involving also other mechanisms, such as macrophage uptake and resulting clearance in the case of anti-inflammatory effects [11], and apoptosis induction in the case of anti-cancer effects [10].

In contrast to the considerable interest that has been devoted to improving AMP potency and selectivity, drug delivery aspects of AMPs have been much less investigated. Yet, AMPs suffer from several challenges in the context of drug delivery, which have to be resolved for AMP therapeutics to reach their full potential. Thus, with the exception of AMPs specifically designed to display stability [8], proteolytic degradation in infected tissue will dramatically reduce the effect of AMPs administered unformulated, e.g., for cystic fibrosis airways, infected mucosal surfaces, or chronic wounds. Here, drug delivery systems may offer approaches for protection of AMPs against proteolytic degradation until they have reached their site of action [12,13]. Furthermore, due to their net positive charge and amphiphilicity, AMPs bind to net anionically charged serum proteins, resulting in rapid clearance from bloodstream circulation and accumulation in the reticuloendothelial system [14,15]. Here, delivery systems may reduce such serum protein binding, as well as scavenging-related activity loss. Delivery systems may also facilitate cell internalization of AMPs, potentially leading to their co-localization with internalized pathogens (important, e.g., for tuberculosis), allowing action of the intracellular bacteria without having to lyse the host macrophages [16]. Furthermore, sustained or triggered AMP release may be of interest, such as for implants or depot formulations against recurring infection. Also here, delivery systems could potentially offer functional advantages for AMP-based therapies [17,18].

Various types of nanomaterials may offer opportunities as delivery systems for AMPs [19], including self-assembly systems formed by surfactants, (block co)polymers, and polar lipids [20–22], polymer (micro)gels [23–25] as well a wide range of inorganic nanoparticles/nanomaterials [12,26–28], each offering system-specific opportunities. Within the present investigation, focus was directed towards microgels as delivery systems for AMPs, as these have previously been demonstrated to be powerful delivery systems for peptides, as well as of other biomacromolecular drugs, including proteins, siRNA, and DNA [29]. Microgels/nanogels are lightly cross-linked polymer colloids, which can be designed to display dramatic swelling/de-swelling in response to various parameters, such as temperature, pH, and ionic strength. In addition, microgels/nanogels can be remotely triggered through external fields, such as near-infrared radiation or light, as well as magnetic field. The responsiveness can also be tuned so that the gels release their cargo on more specific stimuli to certain diseases, e.g., microgels releasing insulin in response to increasing glucose concentration [30], or gels that releases antibiotics in response to bacterial proteases [31].

In order to elucidate key properties of AMP-loaded microgels, we here investigate effects of microgel charge density on AMP loading and release for poly(ethyl acrylate-*co*-methacrylic acid) microgels of different charge density [32], using a method combination of ellipsometry, circular dichroism spectroscopy, nanoparticle tracking analysis, dynamic light scattering, and z-potential measurements. In addition, membrane interactions of peptide-loaded microgels are addressed, and the result correlated to functional consequences, including antimicrobial activity, hemolysis, and proteolytic stability.

2. Materials and methods

2.1. Materials

Peptide AP114 (GFGCNGPWNEDDLRCHNHCKSIKGYKGGY CAKGGFVCKCY, purity 99.1%) was provided by Adenium Biotech ApS (Copenhagen, Denmark), while DPK-060 (GKHKNKGKKNG KHNGWKWWW, purity 98.5%), was synthesized by Bachem AG (Bubendorf, Switzerland) and provided by Pergamum AB (Stockholm, Sweden), LL-37 (LLGDFFRKSKEKIGKEFKRIVQRIKDFLR NLVPRTES, purity 94.7%) was synthesized and provided by PolyPeptide Laboratories (Limhamn, Sweden) and poly-L-lysine (150 kDa, >90% purity) was obtained from Sigma Aldrich (Schnelldorf, Germany). More information on the properties of the antimicrobial peptides used can be found in Table S1, Supporting Information. Lipids DOPE (1,2-dioleoyl-sn-Glycero-3-phos phooethanolamine) and DOPG (1,2-dioleoyl-sn-Glycero-3-phos phglycerol, monosodium salt) (both >99% purity) were obtained from Avanti Polar Lipids (Alabaster, USA). *Escherichia coli (E. coli)* ATCC 25922 was obtained from the American Type Culture Collection, as was *Pseudomonas aeruginosa* (*P. aeruginosa*) ATCC 27853, whereas *Methicillin resistant Staphylococcus aureus* (*MRSA*; clinical strain 0702E0196) and *Pseudomonas aeruginosa* (clinical strain 0704C0134) were isolated from patients at CHU, Angers. Brain-heart infusion (BHI) broth was purchased from bioMérieux (Marcy l'Etoile, France), while Columbia agar plates supplemented with sheep blood were obtained from Oxoid (Dardilly, France). Purified Milli-Q water was used throughout. All other chemicals used were of analytical grade and obtained from Sigma-Aldrich (Schnelldorf, Germany).

2.2. Microgel synthesis

Poly(ethyl acrylate-*co*-methacrylic acid) or poly(ethyl acrylate (EA)/methacrylic acid (MAA)/1,4-butandiol diacrylate (BDDA)) microgels were prepared through seed-feed (starved feed) emulsion polymerization, reported by Rodriguez et al. [33]. The composition of the monomer emulsion feed in w/w was varied to obtain gels with different electrostatic driving forces for peptide adsorption, here either 72.5/26.5/1 or 39/60/1 (EA/MAA/BDDA) w/w was used. Henceforth, microgels are abbreviated according to w/w methacrylic acid content in the feed solution. Titration experiments showed MAA26.5 and MAA60 microgels to have a methacrylic acid content of 34.3 ± 1.1 and 63.3 ± 1.5% w/w, respectively (Table S2, Supporting Information). In the synthesis process, 31.5 g (of the total 260 g) EA/MAA/BDDA monomer mixture was added as a seed to a nitrogen-purged solution consisting of 1.8 g SDS in 517.5 g H_2O under stirring in a four-necked, round-bottom flask at 80 °C. This was immediately followed by addition of dipotassium hydrogen phosphate (3 g of a 7.7 wt% aqueous solution) and ammonium persulfate (APS, 3.6 g of 5 wt%). After 30 min,

the remaining monomer mixture was added continuously (2.6 mL/min) over 90 min. To achieve a similar size range of the microgel systems, a second initiator step (3.2 g of 3 wt% APS) was included in the case of MAA26.5 microgels. During the polymerization process, the size of the microgels was regularly sampled and measured with photon correlation spectroscopy using a BI-9000 Brookhaven light scattering apparatus (Brookhaven Instrument Cooperation, NY, USA), fitted with a 20 mW HeNe laser and the detector set at a 90° scattering angle. When reaching the desired size (≈100 nm diameter), the reaction was stopped by cooling, after which the microgel solution was extensively dialyzed against water.

2.3. Surface preparation and microgel deposition

Silica substrates used were either glass coverslips, 0.16–0.19 mm thickness (Fisher Scientific, Gothenburg, Sweden), or prepared from polished silicon wafers, oxidized to an oxide layer thickness of 30 nm (Semiconductor Wafer Inc., Hsinchu, Taiwan). The resulting silica substrates were cleaned, first in 25% NH_4OH, 30% H_2O_2, and H_2O (1:1:5, w/w), followed by 25% HCl, 30% H_2O_2, and H_2O (1:1:5, w/w), both at 80 °C for 5 min. The surfaces were subsequently washed thoroughly in water and ethanol (99.7%). Samples were then functionalized with (3-glycidyloxypropyltrimethoxysilane (GOPS) to enable microgel immobilization to the surfaces using a slightly modified previously reported protocol by Wong et al. [34]. In short, surface silanol groups were reacted with GOPS, providing a chemical handle for carboxyl functionalities on the microgels to attach to by forming ester bonds. This methodology is well established in literature for covalent reactions, both in general and for covalent reactions in surface modifications [35]. The clean surfaces were placed in dry glassware under N_2 (g). Dry toluene (400 mL), GOPS (100 mL), and Hünig's base (3 mL) was added under N_2 (g). The reaction was refluxed at 110 °C for 24 h. Upon completion, the surfaces were sonicated twice for 15 min in methanol, and subsequently rinsed with dichloromethane followed by diethyl ether. The functionalized substrates were immediately submerged in 0.1% w/w microgel solution, pH 5.1, and incubated overnight at 50 °C. Unbound microgels were rinsed off and samples stored in water until further use.

2.4. Microgel size and charge

Size determination of microgels at different peptide loading was investigated by nanoparticle tracking analysis (NTA), using a NanoSight NS500 (NanoSight Ltd., Amesbury, UK), equipped with a 75 mW laser at 532 nm, and NTA 2.3 analytical software. Within an illumination device mounted under a microscope, particles passing through the beam path were visualized and measured. From the particle displacements, diffusion coefficients of individual particles were obtained, and the size subsequently calculated from the Stokes-Einstein equation. A gel solution with concentration $\approx 10^9$ particles/mL was prepared in filtered Tris (10 mM, pH 7.4) (Whatman Anotop 25, GE Healthcare, Little Chalfont, UK). Peptide (LL-37 or DPK-060) was added to obtain concentrations in the range 0–1 μM. The samples were subsequently mixed at 5 °C overnight to reach saturation and kept cold until measurement. Each concentration was run in triplicate for each combination of gel and peptide. Each sample was run 10 times and the results were pooled into one graph that was fitted using PeakFit v4.12 (SeaSolve Software Inc., Framingham, USA).

Microgel z-potential with and without peptide was determined using a Zetasizer Nano ZSP (Malvern Instruments, Malvern, UK) at a scattering angle of 173°. Peptide (0–100 μM) and gel (100 ppm) samples in Tris (10 mM, pH 7.4) were mixed at 5 °C overnight. Analyses were performed at 25 °C in triplicates n = 10, for each sample.

2.5. CD spectroscopy

Circular dichroism (CD) spectra were measured by a Jasco J-810 Spectropolarimeter (Jasco, Easton, USA). Measurements were performed in duplicate at 37 °C in a 10 mm quartz cuvette under stirring with a peptide concentration of 10 μM in Tris (10 mM, pH 7.4), either in the absence or presence of microgels at 333 ppm. The CD signal at 225 nm was used to calculate the α-helix content, using 100% α-helix and 100% random coil references obtained from 0.133 mM (monomer concentration) poly-L-lysine (M_w = 79 kDa) in 0.1 M NaOH and 0.1 M HCl, respectively. To account for instrumental differences between measurements, background correction was performed routinely by subtraction of the buffer spectra of the corresponding samples in the presence of peptide.

2.6. Liposome leakage

Anionic (DOPE/DOPG 75/25 mol/mol) model liposomes were investigated, frequently used as bacteria membrane models [36]. To obtain lipid films, lipids were dissolved in chloroform (13 mM) and mixed in the desired ratio, after which chloroform was carefully evaporated (rotaevaporation at 60 °C for 45 min, followed by vacuum oven overnight at room temperature). The films were subsequently re-dispersed in Tris (10 mM, pH 7.4), also containing 0.1 M carboxyfluorescein (CF) and 5 mM glucose, to a lipid concentration of 6 mM. The solution was subjected to eight freeze (N_2 (l))-thaw (60 °C) cycles and subsequently extruded (LipoFast, Avestin, Ottawa, USA) through 100 nm polycarbonate filters 30 times. Untrapped CF was removed by gel filtration (Sephadex G-50, GE Healthcare, Uppsala, Sweden) with Tris (10 mM, pH 7.4) as eluent. Liposome membrane disruption was monitored for samples at 520 nm in a SPEX-fluorolog 1650 0.22-m double spectrometer (SPEX Industries, Edison, USA) at 37 °C for 30 min. An absolute leakage scale was obtained by disrupting the liposomes at the end of the experiment by adding 0.8 mM Triton X-100 (Sigma-Aldrich, St. Louis, USA). Measurements were performed in duplicates.

2.7. Ellipsometry

Peptide adsorption to microgel-coated silica wafers (prepared as described above), as well as microgel/AMP interaction with DOPE/DOPG bilayers on silica surfaces was studied *in situ* by null ellipsometry, using an Optrel multiskop ellipsometer (Optrel, Kleinmachnow, Germany) equipped with a 100 mV Ar laser. Measurements were carried out at 532 nm and an angle of incidence 67.66° in a 5 mL cuvette under stirring (300 rpm). In brief, the mean refractive index (n) and thickness (d) of a layer at the surface can be obtained by monitoring the state of polarization of light reflected either with or without peptide in the case of microgels at the surface or peptide adsorption to or lipid desorption from lipid bilayers The mass change (adsorption/desorption) at the surface can then be calculated from

$$\Gamma = \frac{(n - n_0)}{dn/dc} * d$$

where n_0 is the refractive index of the bulk solution and dn/dc is the refractive index increment (taken to be 0.154 cm^3/g). Peptide loading was studied on microgel-coated silica wafers in Tris-HCl (10 mM, pH 7.4). Peptide binding to the microgels were measured by step-wise addition of peptide to the cuvette (0.5, 3.75, 7.5, 15, 30, 60, 80 μM), allowing adsorption to reach saturation for at least 45 min before next addition. All samples were run in duplicate.

For studies of the interaction of peptide-loaded microgels with DOPE/DOPG bilayers, the latter were prepared as described for liposome leakage, but with some modification: (i) Tris (10 mM,

pH 7.4) buffer was used instead of carboxyfluorescein-containing Tris (10 mM, pH 7.4), (ii) after extrusion through 100 nm filters, a second extrusion through 30 nm filter was performed, and (iii) no PD-10 column was used. In order to avoid adsorption of peptide directly at the silica substrate through any defects of the supported lipid layer (surface potential −40 mV, contact angle <10°) [37] poly-L-lysine (150 kDa) was pre-adsorbed from water prior to lipid addition to an amount of 0.045 ± 0.01 mg/m^2, followed by removal of non-adsorbed poly-L-lysine by rinsing with water at 5 mL/min for 20 min [38,39]. Water in the cuvette was then replaced by Tris (10 mM, pH 7.4), which was followed by addition of liposomes in buffer at a lipid concentration of 20 μM and subsequent rinsing with Tris (10 mM, pH 7.4, with 150 mM NaCl) at 5 mL/min for 15 min when the liposome adsorption had stabilized in order to remove non-adsorbed and weakly adsorbed liposomes. Subsequently, peptide-loaded microgels were added at a concentration of 10 ppm microgel with and without 0.3 μM peptide respectively, and the adsorption was monitored over 1 h, followed by rinsing with Tris (10 mM, pH 7.4, with 150 mM NaCl) at 1 mL/min for 30 min and 5 mL/min for an additional 30 min. Duplicate measurements were performed throughout.

2.8. Scanning electron microscopy (SEM) analysis

Gel covered silica wafers were prepared as described above. The surfaces were dried in vacuum and stored under Ar (g). Samples were sputtered with 5 nm platinum before imaging. SEM images were obtained via a Hitachi S-4300 FE-SEM (Tokyo, Japan) at 3 kV.

2.9. Antimicrobial effects

Peptide-microgel formulations were incubated overnight under shaking. Colonies (1–2) were taken directly from Columbia agar plates into 2 ml of 0.85% NaCl solution, and the density of the microorganism suspension adjusted to equal 1.1 McFarland standard (approximately $3.3 \cdot 10^8$ cfu/mL, *MRSA*) or 0.5 McFarland standard ($1.5 \cdot 10^8$ cfu/mL, *P. aeruginosa*, *E. coli*). The bacterial suspensions were further diluted 100 ($3.3 \cdot 10^6$ cfu/mL) or 10 ($1.5 \cdot 10^7$ cfu/mL) times with BHI (AP-114) or water/BHI 100:1 (DPK-060 and LL-37), respectively. An amount of 100 μL of bacterial suspension in BHI or water/BHI 100:1 was added into each well of a sterile 96 well plate already containing 100 μL of peptide, gel or gel-peptide sample. Positive control wells, containing BHI or water/BHI 100:1, and the bacterial suspension without the tested sample (growth control), as well as negative control wells, containing BHI or water/BHI 100:1 and the tested sample without the bacterial suspension (sterility control) were also prepared. The plates were incubated at 37 °C for 24 h. The minimal inhibitory concentration (MIC) was defined as the lowest concentration of the sample that completely inhibited the growth of the bacteria as detected by the unaided eye. If the assessment was not possible due to the turbidity of the sample, an amount of approximately 2 μL was withdrawn from each well, transferred onto a plate with Mueller Hinton agar using an AQS multipoint inoculator and incubated for 24 h at 37 °C. Values reported were determined from triplicate experiments.

2.10. Proteolytic stabilization

Peptide (2 μg) or peptide-microgel formulations were incubated at 37 °C with *P. aeruginosa* elastase (PE, 0.2 μg, 25000 units/mg) (BioCol GmbH, Potsdam, Germany) in a total volume of 15 μL of Tris (10 mM, pH 7.4) for 16 h. The materials were placed on 10–20% precast Tris-Tricine sodium dodecyl sulfate polyacrylamide (SDS-PAGE) Tris-Tricine gels (Invitrogen) and analyzed after staining with Coomassie Brilliant Blue. Quantification of band intensities, from triplicate measurements, was performed by Molecular Imager Gel DOC with Image Lab Software (BioRad, Hercules, USA).

2.11. Hemolysis

EDTA-blood was centrifuged at 800*g* for 10 min, and plasma and buffy coat removed. Erythrocytes were washed three times and re-suspended in 5% PBS, pH 7.4. The cells were then incubated with end-over-end rotation for 1 h at 37 °C in the presence of microgels with or without peptide at the indicated concentrations. For comparison, 2% Triton X-100 (Sigma-Aldrich, St. Louis, USA) served as positive control. The samples were then centrifuged at 800*g* for 10 min. The hemoglobin release was measured by absorbance at 550 nm and is expressed as% of Triton X-100-induced hemolysis (n = 3).

3. Results

3.1. Peptide loading and release

As a consequence of loading of net positively peptide into the negatively charged microgels, the latter display pronounced osmotic de-swelling, as demonstrated for both LL-37 and DPK-060 (Fig. 1). Quantitatively, both MAA26.5 and MAA60 display drastic de-swelling even at low DPK-060, reaching limiting collapse at the lowest concentration used, i.e., at a peptide concentration of 0.0001 μM for a microgel concentration of 10^8 microgels/mL (≈600 peptides/microgel particle, assuming complete peptide binding). For LL-37, both microgels display a more gradual de-swelling with increasing LL-37 concentration. Furthermore,

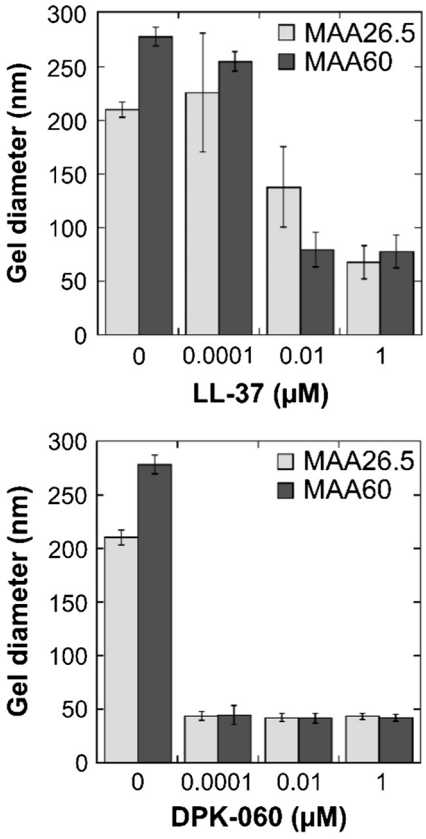

Fig. 1. Microgel de-swelling upon addition of LL-37 or DPK-060 to MAA26.5 or MAA60 microgels in Tris (10 mM, pH 7.4).

the more negatively charged MAA60 reaches limiting collapse at a lower LL-37 concentration than the lower charged MAA26.5. Together, the particle size results thus indicate that while electrostatic interactions are important for peptide loading into the microgels, this also varies between different AMPs, the smaller and slightly higher charged DPK-060 inducing more pronounced de-swelling on microgel loading.

Despite the importance of electrostatic interactions for peptide loading, however, the z-potential of the loaded microgels unexpectedly only changes marginally upon peptide loading up to a peptide concentration of 100 μM (Fig. 2a). Nevertheless, peptide loading results in the formation of oligomers for both microgels, but somewhat more extensively so for DPK-060 (Figs. 2b and S1, Supporting Information). This indicates that the microgel z-potential is dictaded by dilute negatively charged tails, the repulsive barrier is partially overcome after peptide loading as a result of van der Waals interactions (increasing with microgel de-swelling) and potentially also by positively charged patches on the microgel particles.

To quantify peptide loading and binding kinetics further, microgel-covered silica wafers were prepared at a surface coverage of 10–15% ($3–5 \cdot 10^{13}$ microgel particles/m^2) (Fig. 3a and b). As seen in Fig. 3c, ellipsometry shows that background adsorption of the peptides investigated to the underlying surface was quite limited, allowing quantification of peptide loading to the surface-bound microgels. From this, it was found that the surface-bound microgels are able to incorporate considerable amounts of peptide, and that binding displayed high affinity behavior, followed by more gradual binding at higher peptide loads (Fig. S2, Supporting Information). Furthermore, saturation binding of LL-37 and DPK-060 is quite similar, in both cases increasing somewhat with increasing microgel charge density.

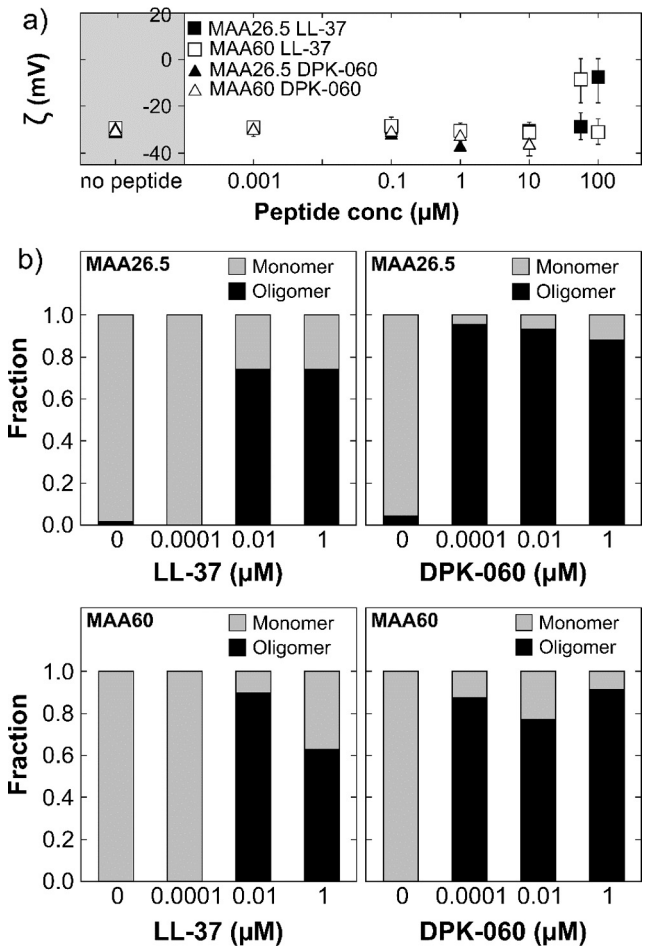

Fig. 2. (a) Z-potential of MAA26.5 and MAA60 microgels in the absence and presence of either LL-37 or DPK-060 at the indicated concentration in Tris (10 mM, pH 7.4). The microgel concentration used was 100 ppm. (b) Fraction of peptide-loaded microgel particles in monomer state. The microgel concentration used was 10^8 particles/mL in Tris (10 mM, pH 7.4).

Following saturation, ellipsometry showed peptide release to be quite limited within the time-frame investigated (2 h) in Tris (10 mM, pH 7.4), for both peptides, whereas peptide release increased in the additional presence of 150 mM NaCl, particularly so for the shorter DPK-060 peptide (Fig. 4). Peptide release was previously found to depend on peptide length [40], net charge, charge distribution, and mean hydrophobicity [41]. It was found that localized charges suppress peptide released due to a locally high charge density, whereas peptide release is facilitated by evenly distributed charges. The present results are in line with these previous findings, as both LL-37 and DPK-060 have quite evenly distributed charges, but LL-37 being substantially longer of the two peptides, thus decreasing its electrolyte-induced release.

As a result of microgel incorporation, LL-37 undergoes considerable conformational changes, from a disordered random coil conformation in aqueous solution, to display pronounced helix formation after microgel incorporation, in analogy to the propensity displayed by this peptide for helix formation after binding to both anionic phospholipid membranes and anionic polysaccharides [42]. Quantitatively, the helix content after microgel binding is independent of gel charge density (Fig. 5). In contrast to the pronounced helix induction observed for LL-37, DPK-060, previously demonstrated to undergo only limited conformational changes on anionic complexation [8], displays a largely disordered structure also after microgel incorporation, again independent of microgel charge density in the range investigated (Fig. 5).

3.2. Membrane interactions

Next, the interaction of MAA26.5 and MAA60 microgels with DOPE/DOPG supported bilayers was investigated. As seen in Fig. 6, the MAA26.5 and MAA60 microgels, both having a z-potential of $z \approx -30$ mV, displayed limited binding to the similarly net negatively charged DOPE/DOPG bilayers (−35 mV), independent of microgel concentration in the range 1–1000 ppm. Preloading the microgels (at a 10 ppm concentration) with LL-37 or DPK-060 at 0.3 μM resulted in some adsorption to the DOPE/DOPG bilayer in the case of LL-37 but less so for DPK-060. Mirroring the lack of adsorption of peptide-void microgels, neither MAA26.5 nor MAA60 caused any liposome leakage induction in DOPE/DOPG liposomes in low ionic strength, up to a microgel concentration of 100 ppm, whereafter some, relatively minor, leakage induction is observed (Fig. 7a). Furthermore, the potent membrane disruption observed for both DPK-060 and LL-37 in solution is essentially lost after incorporation into MAA26.5 or MAA60 microgels (Fig. 7b) in Tris (10 mM, pH 7.4), demonstrating peptide localization into the interior of the microgels, in agreement with the absence of adsorption to supported DOPE/DOPG bilayers at low ionic strengths, as well as the net negative z-potential of the peptide-loaded microgels. Similar effects on liposome leakage and z-potential were observed also for the antimicrobial peptide AP114, as were effects on z-potential for Polymyxin B and poly-L-lysine upon incorporation into microgels (results not shown), demonstrating the generality of these effects for different peptides. After allowing peptide-loaded microgels to release their peptide cargo at higher ionic strength overnight, however, membrane disruption capacity is partially restored, an effect more pronounced for the lower charged MAA26.5 microgels (Fig. 8). Therefore, the membrane-disrupting effect seen for these systems is caused by

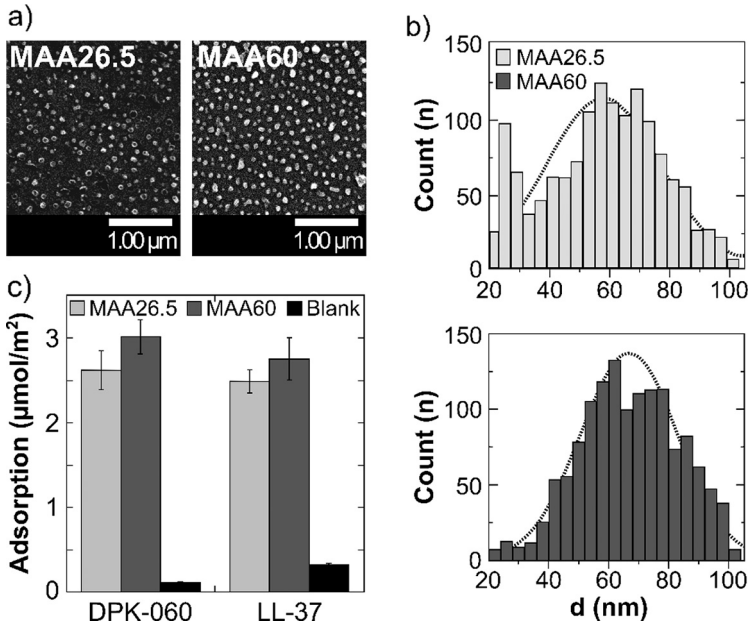

Fig. 3. (a) Representative SEM images of silicon wafers coated with MAA26.5 (left) and MAA60 (right). For both microgels, the gel coverage, batch-to-batch variation included, is 10–15%. (b) The immobilized microgel particles display a wide distribution in size, but are in both cases centered around 70 nm. (c) Saturation binding of LL-37 and DPK-060 to MAA26.5 and MAA60 microgels immobilized on silica substrates from Tris (10 mM, pH 7.4). Background adsorption at the underlying substrate, in the absence of surface-bound microgels, is indicated as well.

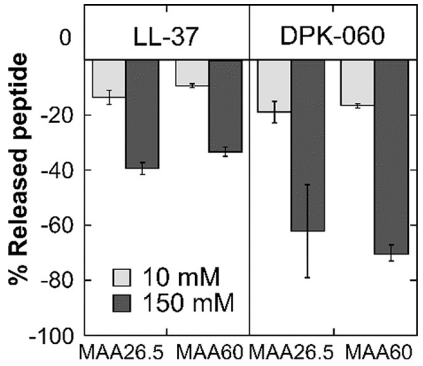

Fig. 4. Ellipsometry results on desorption of microgel-loaded peptides in Tris (10 mM, pH 7.4), with or without additional 150 mM NaCl. Before rinsing, the surface-bound microgels were allowed to reach maximum peptide loading, and stabilize for 2 h. Surfaces were then rinsed at 1 ml/min in a 3 mL cuvette for 2 h under stirring. Increasing the ionic strength triggered peptide release from the microgels.

free peptide released from the microgels, rather than adsorption of a peptide-loaded gel.

3.3. Antimicrobial effects

Having clarified the membrane interactions of the MAA26.5 and MAA60 microgels in the absence and presence of antimicrobial peptide incorporation, we next investigated how the observations made with the model lipid membranes correlated to experiments on bacteria strains. In line with the ellipsometry and liposome leakage results, *in vitro* studies on Gram-negative *E. coli, and P. aeruginosa*, and Gram-positive *MRSA* showed that neither MAA26.5 nor MAA60 display bactericidal effect on its own, MIC being above 100 ppm, the highest microgel concentration investigated (Table 1). Furthermore, antimicrobial effects of DPK-060 were found to be promoted by decreasing microgel charge density, reflecting the faster peptide release of this peptide from MAA26.5 microgels. Quantitatively, the latter resulted in MIC values comparable to that of the free peptide on *E. coli* and *MRSA*. In the case of

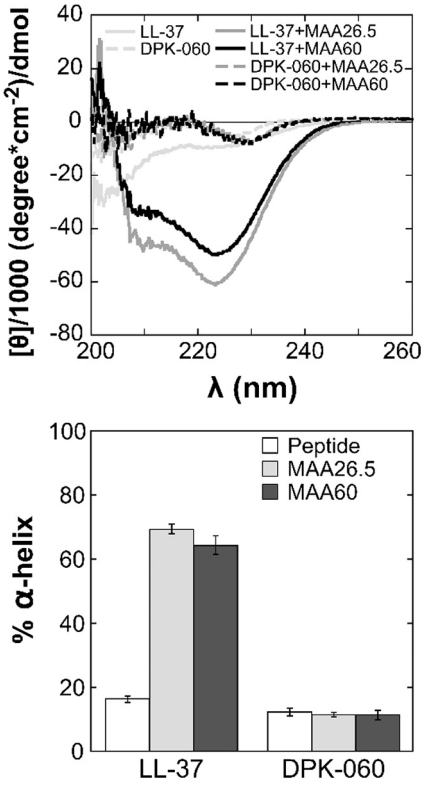

Fig. 5. Circular dichorism spectra (top) and helix content (bottom) of 10 µM LL-37 and DPK-060 before and after peptide loading to MAA26.5 and MAA60 microgels (333 ppm) in Tris (10 mM, pH 7.4).

the two *P. aeruginosa* strains, an improved MIC was observed for the DPK-060-loaded MAA26.5-microgels. For LL-37, displaying slower peptide release, on the other hand, microgel incorporation resulted in a pronounced increase in MIC, reflecting microgel encapsulation of the peptide not released.

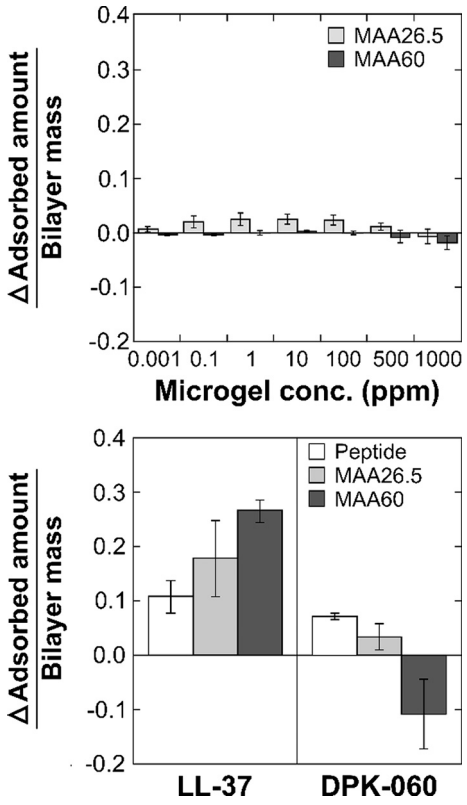

Fig. 6. Normalized microgel binding to supported DOPE/DOPG bilayers in Tris (10 mM, pH 7.4) (above). Relative adsorption change, after bilayer mass normalization, upon addition of MAA26.5 or MAA60 microgels (10 ppm) loaded with LL-37 and DPK-060 at 0.3 μM in Tris (10 mM, pH 7.4) (below). Values reported represent limiting net adsorption differences after 1 h incubation with the bilayer in Tris (10 mM, pH 7.4). For comparison, data obtained for free peptide are included as well.

3.4. Hemolysis

Mirroring the low membrane affinity of empty MAA26.5 and MAA60 microgels, as well as of the corresponding microgels loaded with LL-37 and DPK-060, hemolysis is quite low. Hemolysis shows low erythrocyte destabilization of the empty microgels, close to the negative control, up to microgel concentrations of 100 ppm (Fig. 9a). For microgels loaded with DPK-060, the hemolysis is comparable to that of the free peptide (Fig. 9b), whereas incorporating LL-37 into microgels significantly decreases the hemolysis caused by this peptide, the latter effect slightly more pronounced for the more highly charged MAA60 microgels.

3.5. Proteolytic stabilization

Finally, we note that incorporation into MAA60 offers protection of LL-37 against proteolytic degradation by infection-related enzymes from bacteria (*P. aeruginosa* elastase, PE) (Fig. 10). This is in line with the preferential localization of LL-37 within the microgel particles, demonstrated above, and limited access for the relatively large PE enzymes into the small pores. In contrast, the less charged MAA26.5 microgels do not offer such protection against proteolytic degradation.

4. Discussion

Although microgels have been found to offer advantages as delivery agents of biomacromolecular drugs, including peptides, proteins, DNA, and siRNA [43,44], and although peptide loading and release to/from microgels have been shown to depend on factors such as peptide length [45], hydrophobicity (distribution) [46], charge (distribution) [41], and secondary structure [47], as well as on biodegradation of both peptide [48], and microgel [49], studies of the use of microgels/nanogels as AMP carriers are relatively

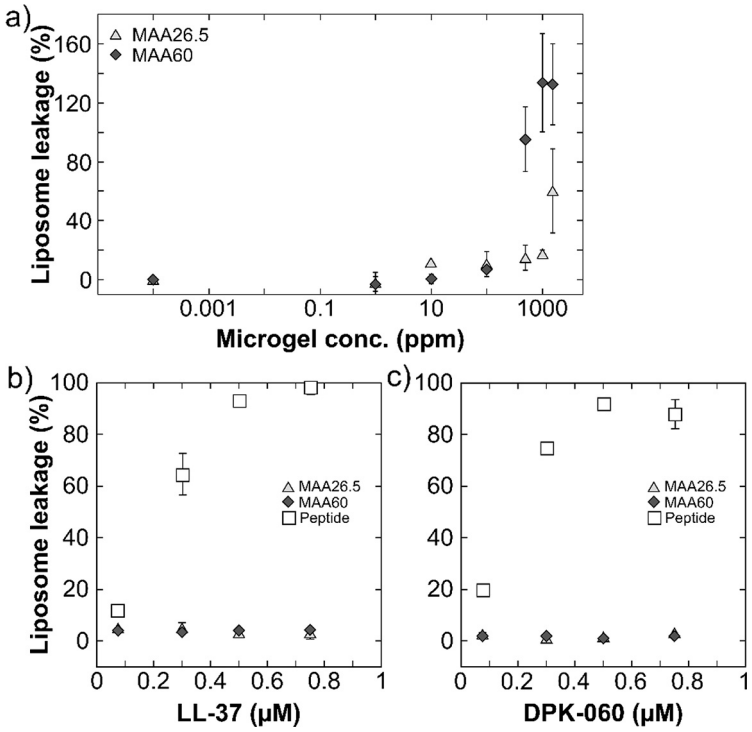

Fig. 7. Leakage of DOPE/DOPG liposomes upon incubation with MAA26.5 and MAA60 microgels (10 ppm) in the absence (a) or presence of either LL-37 (b) or DPK-060 (c).

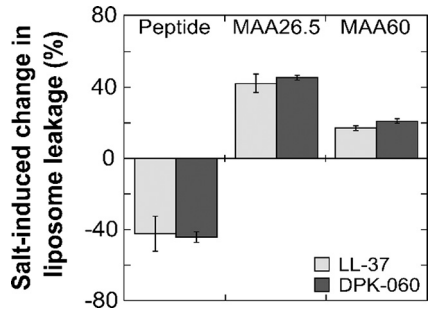

Fig. 8. Comparison between liposome leakage for free peptide at 0.3 μM, with and without 10 ppm MAA26.5 or MAA60. Results are plotted as the difference between leakage at high (Tris 10 mM with 150 mM NaCl) – low (10 mM Tris) ionic strength. A positive value means increased effect at physiological electrolyte concentration. As seen, enhanced membrane disruption is observed for the microgel/peptide systems due to electrolyte-induced peptide release, whereas free peptide in absence of microgel display partial inactivation at high ionic strength.

scarce. However, Water et al. [50] investigated incorporation of novicidin (KNLRRIIRKGIHIIKKYF) in hydrophobically-modified hyaluronic acid-based microgels, and found that both encapsulation efficiency and z-potential could be tuned by changing the preparation parameters, reaching a maximum peptide load of ≈36%. The microgels were found to display good colloidal stability and complete peptide release over 14 days. Furthermore, binding of novicidin to the hyaluronic acid microgels significantly reduced peptide toxicity against HUVECs and NIH 3 T3 cells, while showing no loss of antimicrobial activity against *E. coli* and *S. aureus* [50]. These results are partly in line with those found presently for LL-37 and DPK-060 in poly(ethyl acrylate-*co*-methacrylic acid) microgels, particularly in relation to the long release time of net positively charged AMPs from negatively charged microgels, and regarding the high peptide drug loading reachable with such microgel systems. Having said that, we also note some differences, notably an onset of microgel oligomerization (but at maintained large-scale colloidal stability) at high AMP loads, as well as remaining negative z-potential at high peptide load for the presently investigated poly(ethyl acrylate-*co*-methacrylic acid) microgels. Although the underlying mechanisms behind these differences are difficult to pin-point due to the lack of more systematic studies of peptide loading, detailed studies of particle size distributions, and membrane interactions for the previously reported novocidin/hyaluronic acid microgel study, these likely relate to the higher charge density and smaller persistence length of poly(ethyl acrylate-*co*-methacrylic acid) compared to hyaluronic acid, allowing the formation of dangling tails at the microgel surface.

Somewhat related, Silva et al. investigated loading of LLKKK18 (KEFKRIVKRIKKFLRKLV) into hyaluronic acid microgels in an effort to reach efficient anti-tuberculosis effects [25]. Peptide incorporation into the hyaluronic acid microgels was found to result in increased peptide stability, as also demonstrated in the present investigation for LL-37 loaded onto MAA60 microgels, and reduced cytotoxicity, again in line with findings for LL-37. Importantly, Silva et al. also found microgels to be effectively internalized by macrophages, and the microgel-loaded peptide to co-localize with mycobacteria within host cells. This resulted in a significant reduction of the mycobacterial load in macrophages infected with either *Mycobacterium avium* (*M. avium*) or *Mycobacterium tuberculosis* (*M. tuberculosis*), mirrored by lowered pro-inflammatory cytokine (IL-6 and TNF-α) levels. *In vivo*, intra-tracheal administration of peptide-loaded microgels significantly reduced infection levels in mice challenged by *M. avium* or *M. tuberculosis* after just 5 or 10 every other day administrations [25].

From a mechanistic perspective, a number of interesting effects can be noted from both these previous and the present investigation. Notably, microgels offer opportunities for reaching very high peptide loading, thereby protecting incorporated peptides from proteolytic degradation, depending on the microgel charge densities, and without suffering from large-scale colloidal destabilization. Having said that, the factors determining AMP loading seem to be complex. For example, while increasing microgel net charge increases the driving force for peptide incorporation, peptide binding causes the microgel particles to de-swell osmotically from the surface inwards. In case of too strong peptide-microgel charge contrast, or in the presence of additional strong interactions (e.g., hydrophobic), this de-swelling front can move faster than peptide diffusion, in turn resulting in the formation of a compact shell around each microgel particle [46,41,51]. Such effects have previously been investigated in some detail for larger microgels through confocal microscopy, but are considerably more challenging to monitor directly for microgels as small as those investigated in the present study. Although oligomerization may occur after peptide loading (Fig. S1), peptide-loaded microgels obtain zero charge only at very high peptide concentrations. Correspondingly, initial peptide release, occurring from the outer regions of the microgels, will result in rapid negative zeta poteintial growth of the partially loaded microgels, reducing any tendency of aggregation. Aggregation-induced peptide release is therefore unlikely as a peptide release mechanism in these systems. However, as demonstrated for LL-37, AMPs incorporated into oppositely charged microgels may undergo dramatic conformational changes, likely to affect peptide packing, loading capacity, and subsequent release rate. In analogy to findings for larger microgels, the effect of microgel loading on proteolytic stabilization of incorporated AMPs may depend on microgel charge density (as observed also in the present investigation) also in the absence of shell formation due to tighter peptide binding to the microgel chains, thus precluding access to these also for proteases able to enter into the microgels [48]. Thus, further studies are needed to clarify the details of peptide conformation, as well as radial peptide distribution within the microgel particles, and how this translates into peptide release rate, membrane interactions, and antimicrobial effects. Having said that, it seems clear that peptide release is required for membrane destabilization and antimicrobial effects of anionic microgels, a process suppressed at high microgel charge contrast, as well as for longer

Table 1
Minimal inhibitory concentration (MIC; μM) for free DPK-060 as well as microgel-loaded peptides against *MRSA*, *E. coli*, and two *P. aeruginosa* (PSA) strains.[a]

MIC (μM)	MRSA	E. coli	PSA clin	PSA ATCC
DPK-060	1.6	3.2	6.4	3.2
MAA26.5 + DPK-060	0.8–1.6	1.6–3.2	0.8	0.8
MAA60 + DPK-060	3.2	6.4	6.4	3.2
LL-37	1.8–3.6	3.6	1.8–3.6	1.8–3.6
MAA26.5 + LL-37	>7.1	>7.1	>7.1	7.1
MAA60 + LL-37	>7.1	>7.1	>7.1	>7.1
AP114	4	–	–	–
MAA26.5 + AP114	2–4	–	–	–

[a] Microgel without peptide displays no detectable antimicrobial effect up to at least 100 ppm.

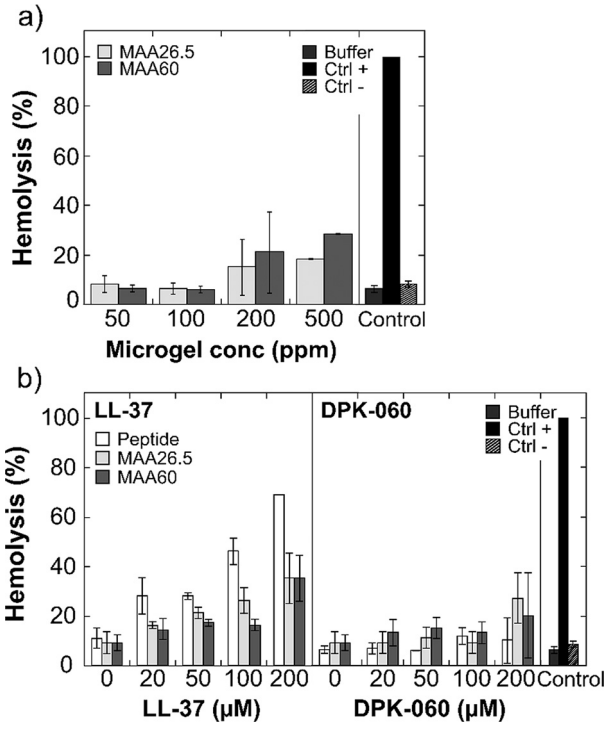

Fig. 9. Effect of microgels, peptides, and peptide-loaded microgels on hemolysis. (a) Hemolysis as a function of microgel (MAA26.5 and MAA60) concentration, performed in 5% PBS, pH 7.4. (b) Hemolysis as a function of LL-37 and DPK-060 concentration with or without 100 ppm microgels MAA26.5 and MAA60, performed in Tris (10 mM pH 7.4) [52].

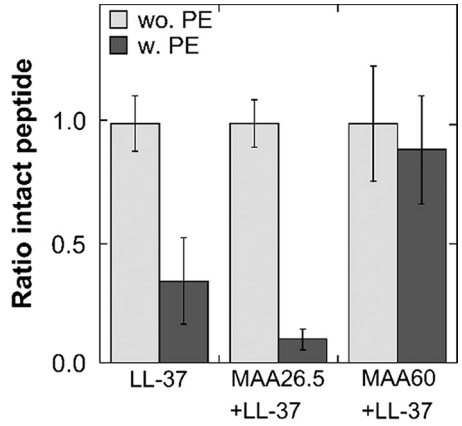

Fig. 10. Ratio intact LL-37 peptide before (wo.) and after (w.) treatment with *pseudomonas elastase* (PE). Loading the peptide onto microgels does not in itself affect the peptide structure.

peptides. As charge contrast is needed for peptide incorporation [43], moderating this in an effort to increase release rate and antimicrobial effects may therefore come at a price of reduced peptide loading capacity. As an alternative approach, biodegradable microgels may offer interesting opportunities in cases where biodegradation can be designed to be slow during storage, but fast or triggered after administration [49].

5. Conclusions

Anionic poly(ethyl acrylate-*co*-methacrylic acid) microgels are able to incorporate considerable amounts of the cationic AMPs LL-37 (LLGDFFRKSKEKIGKEFKRIVQRIKDFLRNLVPRTES) and DPK-060 (GKHKNKGKKNGKHNGWKWWW), the peptides residing primarily inside the microgels, as evidenced by z-potential measurements. As a result of this, incorporated peptides can be protected from degradation by infection-related proteases at high microgel charge densities. Furthermore, as a result of net negative z-potential, also at high peptide load, neither empty nor peptide-loaded microgels adsorb at bacteria-mimicking lipid membranes. Instead, membrane disruption is mediated almost exclusively by peptide release. Analogously, antimicrobial effects require peptide release, and are thus promoted by decreasing peptide length and decreasing microgel charge density. Taken together, the results provide some new insight on microgels as peptide delivery systems [19] through the correlation between peptide loading/release, membrane interactions of void and peptide-loaded microgels, and functional consequences of this in terms of antimicrobial effect, toxicity, and protection from proteolytic degradation.

Acknowledgement

Mrs. Lise-Britt Wahlberg and Dr. Tomas Edvinsson are gratefully acknowledged for technical support and for putting the Zetasizer to our disposal, respectively. Prof. Brian Saunders is gratefully acknowledged for support in relation to microgel synthesis. The research was funded by the European Union's Seventh Framework Program (FP7/2007-2013) under grant agreement no 604182, FORMAMP-Innovative Nanoformulation of Antimicrobial Peptides to Treat Bacterial Infectious Diseases (http://ec.europa.eu.research). All partners in the FORMAMP-project are acknowledged for valuable scientific discussions and input.

Appendix A. Supplementary material

Key properties of microgels and peptides investigated, peptide binding isotherms to surface-bound microgels, liposome leakage studies for AP114 at low ionic strength and for DPK-060, and LL-37 at high ionic strength are available as supporting material. In addition, microgel oligomerization behavior upon peptide loading is exemplified in an NTA-graph. Supplementary data associated with this article can be found, in the online version, at https://doi.org/10.1016/j.jcis.2017.11.014.

References

[1] M. Zasloff, Nature 415 (6870) (2002) 389–395.
[2] R.E.W. Hancock, H.-G. Sahl, Nat. Biotechnol. 24 (12) (2006) 1551–1557.
[3] K.A. Brogden, Nat. Rev. Microbiol. 3 (3) (2005) 238–250.
[4] S.E. Blondelle, K. Lohner, Biopolymers 55 (1) (2000) 74–87.
[5] H. Jenssen, T. Lejon, K. Hilpert, C.D. Fjell, A. Cherkasov, R.E.W. Hancock, Chem. Biol. Drug Des. 70 (2) (2007) 134–142.
[6] M. Pasupuleti, B. Walse, B. Svensson, M. Malmsten, A. Schmidtchen, Biochemistry 47 (35) (2008) 9057–9070.
[7] P. Papareddy, V. Rydengård, M. Pasupuleti, B. Walse, M. Mörgelin, A. Chalupka, M. Malmsten, A. Schmidtchen, PLoS Pathog. 6 (4) (2010) e1000857.
[8] A. Schmidtchen, M. Pasupuleti, M. Mörgelin, M. Davoudi, J. Alenfall, A. Chalupka, M. Malmsten, J. Biol. Chem. 284 (26) (2009) 17584–17594.
[9] A. Schmidtchen, M. Malmsten, Curr. Opin. Colloid Interf. Sci. 18 (5) (2013) 381–392.
[10] D. Gaspar, A.S. Veiga, M.A.R.B. Castanho, Front. Microbiol. 4 (2013) 294.
[11] F.C. Hansen, M. Kalle-Brune, M.J.A. van der Plas, A.-C. Stromdahl, M. Malmsten, M. Morgelin, A. Schmidtchen, J. Immunol. 194 (11) (2015) 5397–5406.
[12] K. Braun, A. Pochert, M. Lindén, M. Davoudi, A. Schmidtchen, R. Nordström, M. Malmsten, J. Colloid Interf. Sci. 475 (2016) 161–170.
[13] A.K. Tiwari, V. Gajbhiye, R. Sharma, N.K. Jain, Drug Deliv. 17 (8) (2010) 605–616.
[14] F.M. Veronese, A. Mero, BioDrugs 22 (5) (2008) 315–329.
[15] G. Sahay, D.Y. Alakhova, A.V.J. Kabanov, Control. Release 145 (3) (2010) 182–195.
[16] B.C. VanderVen, R.J. Fahey, W. Lee, Y. Liu, R.B. Abramovitch, C. Memmott, A.M. Crowe, L.D. Eltis, E. Perola, D.D. Deininger, T. Wang, C.P. Locher, D.G. Russell, PLoS Pathog. 11 (2) (2015) e1004679.
[17] L. Zhang, D. Pornpattananangkul, C.-M.J. Hu, C.-M. Huang, Curr. Med. Chem. 17 (2010) 585–594.

[18] S. Sandreschi, A.M. Piras, G. Batoni, F. Chiellini, Nanomedicine 11 (13) (2016) 1729–1744.
[19] R. Nordström, M. Malmsten, Adv. Colloid Interf. Sci. 242 (2017) 17–34.
[20] L. Boge, H. Bysell, L. Ringstad, D. Wennman, A. Umerska, V. Cassisa, J. Eriksson, M.L. Joly-Guillou, K. Edwards, M. Andersson, Langmuir 32 (17) (2016) 4217–4228.
[21] M. Fumakia, E.A. Ho, Mol. Pharm. 13 (7) (2016) 2318–2331.
[22] S. Mizukami, M. Hosoda, T. Satake, S. Okada, Y. Hori, T. Furuta, K. Kikuchi, J. Am. Chem. Soc. 132 (28) (2010) 9524–9525.
[23] P. Dong, Y. Zhou, W. He, D.B. Hua, Chem. Commun. 52 (5) (2016) 896–899.
[24] R.T.C. Cleophas, J. Sjollema, H.J. Busscher, J.A.W. Kruijtzer, R.M.J. Liskamp, Biomacromolecules 15 (9) (2014) 3390–3395.
[25] J.P. Silva, C. Gonçalves, C. Costa, J. Sousa, R. Silva-Gomes, A.G. Castro, J. Pedrosa, R. Appelberg, F.M. Gama, J. Control. Release 235 (2016) 112–124.
[26] M. Malmsten, Curr. Opin. Colloid Interf. Sci. 18 (5) (2013) 468–480.
[27] W.-Y. Chen, H.-T.H.-Y. Chang, J.-K. Lu, Y.-C. Huang, S.G. Harroun, Y.-T. Tseng, Y.-J. Li, C.-C. Huang, H.-T.H.-Y. Chang, Adv. Funct. Mater. 25 (46) (2015) 7189–7199.
[28] A. Sur, B. Pradhan, A. Banerjee, P. Aich, PLoS One 10 (4) (2015) e0123905.
[29] H. Bysell, R. Månsson, P. Hansson, M. Malmsten, Adv. Drug Deliv. Rev. 63 (13) (2011) 1172–1185.
[30] K. Kataoka, H. Miyazaki, M. Bunya, T. Okano, Y. Sakurai, J. Am. Chem. Soc. (1998) 12694–12695.
[31] M.-H. Xiong, Y.-J. Li, Y. Bao, X.-Z. Yang, B. Hu, J. Wang, Adv. Mater. 24 (46) (2012) 6175–6180.
[32] L. Nyström, R. Alvarez-Asencio, G. Frenning, B.R. Saunders, M.W. Rutland, M. Malmsten, ACS Appl. Mater. Interf. 8 (40) (2016) 27129–27139.
[33] B.E. Rodriguez, M.S. Wolfe, M. Fryd, Macromolecules 27 (22) (1994) 6642–6647.
[34] A.K.Y. Wong, U.J. Krull, Anal. Bioanal. Chem. 383 (2) (2005) 187–200.
[35] W.J. Blank, Z.A. He, M.J. Picci, Coatings Technol. 74 (3) (2002) 33–41.
[36] A.A. Strömstedt, L. Ringstad, A. Schmidtchen, M. Malmsten, Curr. Opin. Colloid Interf. Sci. 15 (6) (2010) 467–478.
[37] M. Malmsten, N. Burns, A. Veide, J. Colloid Interf. Sci. 204 (204) (1998) 104–111.
[38] L. Ringstad, A. Schmidtchen, M. Malmsten, Langmuir 22 (11) (2006) 5042–5050.
[39] L. Ringstad, E. Protopapa, B. Lindholm-Sethson, A. Schmidtchen, A. Nelson, M. Malmsten, Langmuir 24 (1) (2008) 208–216.
[40] H. Bysell, A. Schmidtchen, M. Malmsten, Biomacromolecules 10 (8) (2009) 2162–2168.
[41] H. Bysell, P. Hansson, M. Malmsten, J. Phys. Chem. B 114 (21) (2010) 7207–7215.
[42] U.H.N. Dürr, U.S. Sudheendra, A. Ramamoorthy, Biochim. Biophys. Acta - Biomembr. (2006) 1408–1425.
[43] M. Malmsten, H. Bysell, P. Hansson, Curr. Opin. Colloid Interf. Sci. 15 (6) (2010) 435–444.
[44] L. Nyström, M. Malmsten, Adv. Colloid Interf. Sci. (2016) 88–104.
[45] H. Bysell, M. Malmsten, Langmuir 22 (12) (2006) 5476–5484.
[46] H. Bysell, P. Hansson, A. Schmidtchen, M. Malmsten, J. Phys. Chem. B 114 (3) (2010) 1307–1313.
[47] R. Månsson, H. Bysell, P. Hansson, A. Schmidtchen, M. Malmsten, Biomacromolecules 12 (2) (2011) 419–424.
[48] R. Månsson, G. Frenning, M. Malmsten, Biomacromolecules 14 (7) (2013) 2317–2325.
[49] R. Widenbring, G. Frenning, M. Malmsten, Biomacromolecules 15 (10) (2014) 3671–3678.
[50] J.J. Water, Y. Kim, M.J. Maltesen, H. Franzyk, C. Foged, H.M. Nielsen, Pharm. Res. 32 (8) (2015) 2727–2735.
[51] H. Bysell, M. Malmsten, Langmuir 25 (1) (2008) 522–528.
[52] J. Kyte, R.F. Doolittle, J. Mol. Biol. 157 (1) (1982) 105–132.